HOKKAIDO UNIVERSITY

Title	Eddy Current Analysis of Litz Wire Considering Circulating Currents Using Integral Equations
Author(s)	Hada, Naoki; Hiruma, Shingo; Ida, Shoma et al.
Citation	IEEE transactions on magnetics https://doi.org/10.1109/TMAG.2026.3735702
Issue Date	2026-09-21
Doc URL	https://hdl.handle.net/2115/100418
Rights	© 2026 IEEE. Personal use of this material is permitted. Permission from IEEE must be obtained for all other uses, in any current or future media, including reprinting/republishing this material for advertising or promotional purposes, creating new collective works, for resale or redistribution to servers or lists, or reuse of any copyrighted component of this work in other works.
Type	journal article
File Information	IEEE Trans. Magn.20260921.pdf

Hokkaido University Collection of Scholarly and Academic Papers : HUSCAP

Eddy Current Analysis of Litz Wire Considering Circulating Currents Using Integral Equations

Naoki Hada[1], Shingo Hiruma[1], Shoma Ida[2], Nobutaka Onishi[2], and Masanao Yamashita[2]
[1]Graduate School of Information Science and Technology, Hokkaido University, Sapporo 060-0814, Japan
[2]Analysis Technology Research Center, Sumitomo Electric Industries, Ltd., Osaka 554-0024, Japan

This paper presents a voltage excitation formulation of the integral equation method (IEM) for Litz wire analysis with circulating currents and a uniform external magnetic field. A strand-level impedance matrix is assembled from voltage responses to unit current excitations, and the strand currents are obtained by solving terminal circuit equations. The external magnetic field is introduced through voltage sources assigned to each strand and a source term in the magnetization equation. The formulation is validated using a four-conductor model by comparison with FEM. It is then applied to a 49-strand Litz wire model to demonstrate its applicability to 3-D twisting structures. The results show that the twisting level required to suppress loss depends on the excitation mechanism.

***Index Terms*—Circulating currents, eddy current, external magnetic field, integral equation method, litz wire, voltage excitation.**

I. Introduction

THE trend toward higher frequencies and power densities in power electronics has made the evaluation of AC losses in magnetic component windings increasingly important [1], [2]. Litz wires are widely used to reduce skin- and proximity-effect losses [1]. However, practical twisting imperfections can cause imbalances in flux linkage and strand impedance, producing circulating currents and additional losses among strands shorted at the terminals [1], [2]. External magnetic fields can be generated by surrounding winding currents and modified by magnetic cores and air gaps, thereby influencing proximity and circulating current losses in Litz wires [1], [3].

The conventional finite element method (FEM) is widely used for analysis of eddy current losses in Litz wires. However, treating many strands individually requires fine discretization of each strand cross section, resulting in high computational cost [2], [4]. Circuit based approaches, including PEEC/SEEC based methods and equivalent circuit models considering the paths of all strands, have been developed to evaluate nonuniform strand-current distributions and circulating current losses in Litz wires [1], [3], [5]. However, the proximity-effect loss inside each strand cross section is usually evaluated separately by analytical or postprocessing models. Homogenization-based FEM using complex permeability can account for proximity-effect eddy currents and has also been coupled with circuit equations [2]. Nevertheless, proximity-effect magnetization and circulating currents have not been directly coupled in a strand-level IEM formulation for the actual 3-D strand paths.

To reduce the computational cost of 3-D Litz-wire analysis, a fast analysis method based on the integral equation method (IEM) has been proposed, in which each strand is modeled as a 1-D polygonal line and proximity-effect eddy currents are represented using complex permeability [6]. This method avoids fine discretization of strand cross sections and can be linked with field formulations for magnetic cores or homogenized FEM analyses [6], [7]. However, existing IEM-based formulations do not explicitly assemble a strand-level impedance matrix or directly solve terminal circuit equations for circulating currents among shorted strands.

This paper extends the method in [6] by a voltage excitation formulation that explicitly constructs a strand-level impedance matrix accounting for electromagnetic coupling between strands and directly solves the coupled circuit equations. A uniform external magnetic field is also incorporated through strand-wise induced voltage sources and an external-field source term in the IEM magnetization equation. The formulation is validated using a four-conductor model and then applied to a 49-strand Litz-wire model.

II. Formulation

A. Integral Equation Model for Litz Wires

Following [6], the Litz wire domain Ω_c is modeled as a set of 1-D polygonal lines. The domain is discretized into line segments, and a constant complex magnetization vector $\boldsymbol{M}$ is assigned to each segment to represent the anti-parallel eddy currents induced by the proximity effect. The vector satisfies

$$\frac{\boldsymbol{M}(\boldsymbol{x})}{\dot{\mu}_r - 1} = \boldsymbol{\tau} \times \left[\left(\int_{\Omega_\mathrm{c}} \boldsymbol{F}(\boldsymbol{x}, \boldsymbol{x}') \, \mathrm{d}\boldsymbol{x}' + \boldsymbol{H}_0(\boldsymbol{x}) \right) \times \boldsymbol{\tau} \right] , \quad (1)$$

$$\boldsymbol{F}(\boldsymbol{x}, \boldsymbol{x}') = -\frac{1}{4\pi} \left[\frac{\boldsymbol{M}(\boldsymbol{x}')}{R^3} - 3\frac{(\boldsymbol{M}(\boldsymbol{x}') \cdot \boldsymbol{R})\boldsymbol{R}}{R^5} \right] . \quad (2)$$

Here, $\boldsymbol{x}$ and $\boldsymbol{x}'$ denote the observation and source points in Ω_c, respectively, $\boldsymbol{\tau}$ is the unit tangent vector at $\boldsymbol{x}$, $\boldsymbol{R} = \boldsymbol{x} - \boldsymbol{x}'$ and $R = |\boldsymbol{R}|$. The field $\boldsymbol{H}_0$ is generated by the strand currents and is evaluated using the Biot–Savart law. The complex relative permeability $\dot{\mu}_r$ is derived using Bessel functions and accounts for the proximity effect within the strand without fine discretization of the strand cross section [6], [8].

To construct the impedance matrix, unit current excitations are applied strand by strand. For the j-th unit-current excitation, $I_j = 1$ A and $I_k = 0$ for $k \neq j$ are imposed. Under this condition, (1) and (2) are solved to obtain the

The authors declare no conflicts of interest. Corresponding author: S. Hiruma (e-mail: hiruma@ist.hokudai.ac.jp).

complex magnetization distribution $\boldsymbol{M}$. Using the complex power relation in [6], the terminal voltage of strand i is evaluated as

$$V_i = \mathrm{j}\omega \int_{\Omega_{\mathrm{c},i}} \boldsymbol{A}(\boldsymbol{x}) \cdot \boldsymbol{j}_i(\boldsymbol{x})\, \mathrm{d}\boldsymbol{x} + \frac{R_{0,i} z J_0(z)}{2J_1(z)} I_i \,, \tag{3}$$

where j denotes the imaginary unit, ω is the angular frequency, $\Omega_{\mathrm{c},i}$ is the domain of strand i, and $\boldsymbol{A}(\boldsymbol{x})$ is the magnetic vector potential generated by the currents and the complex magnetization $\boldsymbol{M}$. Here, $\boldsymbol{j}_i(\boldsymbol{x})$ denotes the current density distribution in strand i corresponding to a unit current of 1 A flowing in that strand, $R_{0,i}$ is the dc resistance of strand i, and z is a parameter related to the skin depth. The second term represents the internal-impedance voltage drop including the skin effect using Bessel functions J_0 and J_1 [6], [8], [9]. For the j-th excitation, this term contributes only when $i = j$.

The voltage vector $\boldsymbol{V}$ obtained from (3) gives the j-th column of the impedance matrix.

$$Z_{ij} = \left. \frac{V_i}{I_j} \right|_{I_j=1,\ I_k=0\ (k\neq j)} . \tag{4}$$

Repeating this procedure for all strands yields the strand-level impedance matrix $\boldsymbol{Z}$.

When a common terminal voltage V_{app} is applied to the strands without an external magnetic field, the strand currents are obtained from

$$\boldsymbol{Z}\boldsymbol{I} = V_{\mathrm{app}} \mathbf{1} \,, \tag{5}$$

where $\mathbf{1} = [1, 1, \ldots, 1]^{\mathrm{T}}$. The resulting current distribution can include circulating currents caused by imbalance in the electromagnetic coupling between strands.

After the strand currents are determined, the current distribution is used to evaluate the AC loss. Following [6], the complex power of the whole Litz wire system is evaluated as

$$\dot{P} = \sum_{i=1}^{N_{\mathrm{s}}} \left[\frac{\mathrm{j}\omega}{2} \int_{\Omega_{\mathrm{c},i}} \boldsymbol{A}(\boldsymbol{x}) \cdot \boldsymbol{J}_i^*(\boldsymbol{x})\ \mathrm{d}\boldsymbol{x} + \frac{R_{0,i} z J_0(z)}{4J_1(z)} |I_i|^2 \right] . \tag{6}$$

Here, N_{s} is the number of strands, * denotes complex conjugation, and $\boldsymbol{J}_i(\boldsymbol{x}) = I_i \boldsymbol{j}_i(\boldsymbol{x})$ is the current density associated with the solved current I_i in strand i. The AC loss is obtained as $\mathrm{Re}[\dot{P}]$.

Since $\boldsymbol{Z}$ is constructed from current excitations only, external-field effects are treated as right-hand-side source terms.

B. Introduction of External Magnetic Field

The overall longitudinal direction of the Litz wire is taken as the x-axis with unit vector $\boldsymbol{e}_x$, and the transverse cross section is defined as the y-z plane. A spatially uniform transverse external flux density is expressed as $\boldsymbol{B}_{\mathrm{ext}} = [0, B_y, B_z]^{\mathrm{T}}$, and $\boldsymbol{H}_{\mathrm{ext}} = \boldsymbol{B}_{\mathrm{ext}}/\mu_0$. The terminal connections are assumed to lie in equipotential transverse y-z planes at constant x. The detailed geometry of the end connections, which may affect the end-region flux linkage and circulating-current distribution, is not considered in the present model. Under this assumption, the following x-directed vector potential is used

$$\boldsymbol{A}_{\mathrm{ext}}(\boldsymbol{r}) = (B_y z - B_z y)\, \boldsymbol{e}_x \,, \tag{7}$$

which satisfies $\nabla \times \boldsymbol{A}_{\mathrm{ext}} = \boldsymbol{B}_{\mathrm{ext}}$. Since $\boldsymbol{A}_{\mathrm{ext}}$ is x-directed whereas the terminal path elements lie in transverse y-z planes, $\boldsymbol{A}_{\mathrm{ext}} \cdot \mathrm{d}\boldsymbol{\ell} = 0$ on the terminal connections. For segment m, let $\boldsymbol{r}_{m,\mathrm{c}}$ denote its midpoint position vector, $\boldsymbol{\tau}_m$ its unit tangent vector, and $\Delta\ell_m$ its length. The tangential component of the vector potential is $\boldsymbol{A}_{\mathrm{ext}}(\boldsymbol{r}_{m,\mathrm{c}}) \cdot \boldsymbol{\tau}_m = A_{\mathrm{ext},x}(\boldsymbol{r}_{m,\mathrm{c}})(\boldsymbol{e}_x \cdot \boldsymbol{\tau}_m)$. Defining the signed x-component of segment m as $\Delta x_m = (\boldsymbol{e}_x \cdot \boldsymbol{\tau}_m)\Delta\ell_m$, the direct external voltage source is evaluated as

$$V_{i,\mathrm{ext}}^{A} = -\mathrm{j}\omega \sum_{m\in\mathcal{S}_i} A_{\mathrm{ext},x}(\boldsymbol{r}_{m,\mathrm{c}}) \Delta x_m \,, \tag{8}$$

where $\mathcal{S}_i$ is the set of line segments belonging to strand i.

The external magnetic field also induces a proximity-effect magnetization in the strand cross sections. In the present IEM, only the magnetic field component perpendicular to the local strand axis contributes to the anti-parallel eddy currents [6], [7]. For segment m, this component is obtained by

$$\boldsymbol{H}_{\mathrm{ext},m}^{\perp} = \boldsymbol{H}_{\mathrm{ext}} - (\boldsymbol{H}_{\mathrm{ext}} \cdot \boldsymbol{\tau}_m)\boldsymbol{\tau}_m \,. \tag{9}$$

This projection is independent of the sign of $\boldsymbol{\tau}_m$. Equivalently, this projection is applied by the transverse projection operator in (1). Let $\boldsymbol{H}_{\mathrm{current}}$ denote the magnetic field generated by the strand currents and evaluated by the Biot–Savart law. In the presence of the external magnetic field, the source field in (1) is replaced by

$$\boldsymbol{H}_0(\boldsymbol{x}) = \boldsymbol{H}_{\mathrm{current}}(\boldsymbol{x}) + \boldsymbol{H}_{\mathrm{ext}}. \tag{10}$$

Since the integral equation is linear with respect to the source magnetic field, the magnetization response can be decomposed into

$$\boldsymbol{M} = \boldsymbol{M}_{\mathrm{current}} + \boldsymbol{M}_{\mathrm{ext}}. \tag{11}$$

Here, $\boldsymbol{M}_{\mathrm{current}}$ is the response to $\boldsymbol{H}_{\mathrm{current}}$ and is already included in the impedance matrix through the unit current excitations, whereas $\boldsymbol{M}_{\mathrm{ext}}$ is the response to $\boldsymbol{H}_{\mathrm{ext}}$. Therefore, only $\boldsymbol{M}_{\mathrm{ext}}$ is used to evaluate the magnetization-induced voltage source $\boldsymbol{V}_{\mathrm{ext}}^{M}$, avoiding double counting of the current-induced reaction field.

The vector potential generated by this magnetization is

$$\boldsymbol{A}_{\mathrm{ext}}^{M}(\boldsymbol{x}) = \frac{\mu_0}{4\pi} \int_{\Omega_{\mathrm{c}}} \frac{\boldsymbol{M}_{\mathrm{ext}}(\boldsymbol{x}') \times \boldsymbol{R}}{R^3}\, \mathrm{d}\boldsymbol{x}' \,, \tag{12}$$

where $\boldsymbol{R} = \boldsymbol{x} - \boldsymbol{x}'$ and $R = |\boldsymbol{R}|$. The corresponding source vector $\boldsymbol{V}_{\mathrm{ext}}^{M}$ is obtained as the negative voltage drop associated with $\boldsymbol{A}_{\mathrm{ext}}^{M}$ in the first term of (3). With the sign convention used for $\boldsymbol{V}_{\mathrm{ext}}^{A}$ and $\boldsymbol{V}_{\mathrm{ext}}^{M}$, the circuit equation is $\boldsymbol{Z}\boldsymbol{I} = V_{\mathrm{app}}\mathbf{1} + \boldsymbol{V}_{\mathrm{ext}}^{A} + \boldsymbol{V}_{\mathrm{ext}}^{M}$. Here, $\boldsymbol{V}_{\mathrm{ext}}^{A}$ and $\boldsymbol{V}_{\mathrm{ext}}^{M}$ are strand-wise source vectors whose components generally differ among strands, while $\boldsymbol{H}_{\mathrm{ext}}$ enters the magnetization equation through (10).

To isolate the external-field effect, $V_{\mathrm{app}} = 0$ and $\mathbf{1}^{\mathrm{T}}\boldsymbol{I} = 0$ are imposed while circulating currents are allowed. Introducing an unknown common voltage shift V_{c} yields

$$\begin{bmatrix} \boldsymbol{Z} & -\mathbf{1} \\ \mathbf{1}^{\mathrm{T}} & 0 \end{bmatrix} \begin{bmatrix} \boldsymbol{I} \\ V_{\mathrm{c}} \end{bmatrix} = \begin{bmatrix} \boldsymbol{V}_{\mathrm{ext}}^{A} + \boldsymbol{V}_{\mathrm{ext}}^{M} \\ 0 \end{bmatrix} . \tag{13}$$

In the computation, $\boldsymbol{Z}$ is first constructed without the external field. Both $\boldsymbol{V}_{\mathrm{ext}}^{A}$ and $\boldsymbol{V}_{\mathrm{ext}}^{M}$ are then evaluated to solve the circuit equation, after which the magnetization is recomputed

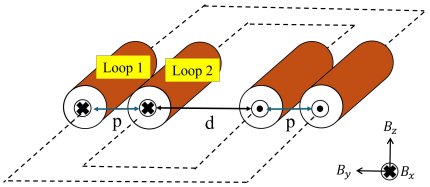

Fig. 1. Four-conductor validation model. Each conductor has radius 1.0 mm and length $L = 1000$ mm. The center-to-center distance between the two conductors on each side is fixed at $p = 2.03$ mm, whereas the center-to-center distance d between the two inner conductors is varied.

using both the current and external-field excitations for loss evaluation.

C. Current Density Reconstruction

For visualization, the strand-wise current density was reconstructed from the solved strand current and segment magnetization as

$$J_{\tau,i}(r,\hat{\boldsymbol{r}}) = \frac{I_i k J_0(kr)}{2\pi a J_1(ka)} + C_{\mathrm{p}} J_1(kr)\left[(\hat{\boldsymbol{r}} \times \boldsymbol{B}_{\mathrm{eq},i}) \cdot \boldsymbol{\tau}_i\right] , \tag{14}$$

$$\boldsymbol{B}_{\mathrm{eq},i} = \mu_0 \frac{\dot{\mu}_r + 1}{2(\dot{\mu}_r - 1)} \boldsymbol{M}_i ,$$

$$C_{\mathrm{p}} = \frac{2\mathrm{j}\omega\sigma a}{J_1(ka) + [kaJ_0(ka) - J_1(ka)]/\mu_r} .$$

Here, a is the strand radius, I_i is the solved current of strand i, $\boldsymbol{\tau}_i$ is the local strand-axis unit vector with the same orientation as the circuit current, $\hat{\boldsymbol{r}}$ is the radial unit vector in the strand cross section, σ and μ_r are the conductivity and relative permeability of the strand material, respectively, and $k = \sqrt{-\mathrm{j}\omega\sigma\mu_0\mu_r}$. The reconstruction follows the circular-wire Bessel solution and complex-permeability relation in [8]. The plotted current-density maps show the magnitude of $J_{\tau,i}$ in A/mm^2.

III. Numerical Results

A. Validation Using a Four-Conductor Model

The voltage excitation formulation was compared with a 2-D FEM model constructed using the commercial software JMAG, as shown in Fig. 1. The model consists of four parallel conductors forming two closed loops. In both models, the two loops were connected in parallel and their common terminal voltage was set to 1 V for the voltage excitation validation and 0 V for the external-field validation. Table I compares resistance and inductance at 9.8 kHz for three values of d. The errors decrease as d increases, suggesting that the proposed formulation reproduces the electromagnetic coupling more accurately as the forward and return conductors become farther apart and the field variation across each conductor decreases.

The conductor loss at 9.8 kHz under uniform 1-mT external magnetic fields in the y- and z-directions was compared with JMAG, as summarized in Table II. Since the loops lie in the x-y plane at $z = 0$, a B_y field does not link the loops and $\boldsymbol{V}_{\mathrm{ext}}^A$ in (8) vanishes, resulting in small errors for all values of d. In contrast, a B_z field links the loop area and produces a differential component of $\boldsymbol{V}_{\mathrm{ext}}^A$, whose magnitude

TABLE I
Voltage Excitation Validation Against 2-D FEM

d [mm]	R_{IEM} [mΩ]	R_{FEM} [mΩ]	Err. [%]	L_{IEM} [μH/m]	L_{FEM} [μH/m]	Err. [%]
20	7.270	6.931	4.9	1.223	1.125	8.6
100	7.078	6.866	3.1	1.807	1.740	3.8
200	7.045	6.864	2.6	2.043	2.013	1.5

TABLE II
External-Field Validation Against 2-D FEM

Field	d [mm]	P_{IEM} [W]	P_{FEM} [W]	Err. [%]
B_y	20	0.194	0.195	0.21
B_y	100	0.195	0.195	0.20
B_y	200	0.195	0.195	0.20
B_z	20	1.322	1.501	11.9
B_z	100	11.431	11.984	4.61
B_z	200	34.533	34.712	0.52

is $|\Delta V_{\mathrm{ext}}^A| = \omega |B_z| L d$. For the B_z case, the error decreases as d increases. This tendency may reflect the cross-sectionally uniform magnetization assumed in the IEM, as the field variation across each conductor becomes weaker for larger d.

B. Demonstration Using a 49-Strand Litz-Wire Model

The proposed method was applied to three 49-strand Litz-wire geometries based on the lw1 model in [3]. Each geometry consists of seven bundles each containing seven strands. The strand diameter, outer diameter, analyzed length, and conductivity were 0.1 mm, 1.0 mm, 30 mm, and 5.98×10^7 S/m, respectively. Each strand was divided into 30 segments. The three geometries were no twist, single-level twist with a 15-mm pitch, and two-level twist with 15- and 30-mm pitches.

First, common terminal voltage excitation was analyzed without an external magnetic field. Because the system is linear, the plotted current-density distributions were normalized to a total current of 1 A for comparison with the current-excited lw1 model reported in [3]. Fig. 2 shows the current density distributions of the two-level twist model at 10 and 100 kHz. At 10 kHz, the current density is nearly uniform among the strands. At 100 kHz, the outer bundles carry larger current densities than the inner bundle, showing a bundle-scale current imbalance. This result is consistent with [3] and shows that the formulation represents both strand-level proximity effect through magnetization and circulating currents through the circuit equation. Fig. 3 shows the AC resistance under 1 V excitation without an external field. The AC resistance was evaluated from the active power and the total terminal current as $R_{\mathrm{ac}} = 2\mathrm{Re}[\dot{P}]/|I_{\mathrm{tot}}|^2$, where peak value phasors are used. The no twist model exhibits a larger AC resistance in the main transition region, whereas the single- and two-level twist models show similar values. This suggests that the first twisting level suppresses most of the strand-scale imbalance associated with the AC resistance under common-terminal voltage excitation. On a workstation with two Intel Xeon Gold 6244 CPUs and 384 GB of memory, the two-level model at 100 kHz required 116.9 s in total, including 113.8 s to construct $\boldsymbol{Z}$ and 0.0021 s to factorize the 49×49 terminal matrix, with a peak memory usage of 303 MiB.

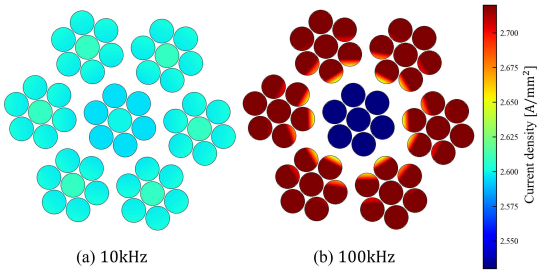

Fig. 2. Reconstructed current-density distributions of the two-level twisted lw1 model under common-terminal voltage excitation without an external magnetic field. The results are normalized to a total current of 1 A.

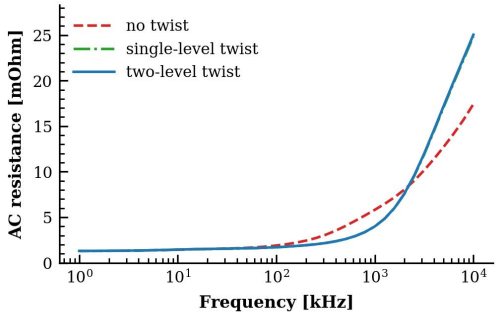

Fig. 3. AC resistance under 1-V excitation without an external magnetic field.

Next, the response to a uniform 1-mT peak external field in the $-z$ direction was investigated under $V_{\mathrm{app}} = 0$ and $\mathbf{1}^{\mathrm{T}}\boldsymbol{I} = 0$. Thus, the computed currents represent external-field-induced circulating currents rather than terminal current excitation. Fig. 4 shows the AC loss under the uniform 1-mT external magnetic field in the $-z$ direction. At 100 kHz, $\mathrm{Re}[\dot{P}]$ is 2.186 mW without twisting, 1.891 mW with single-level twisting, and 0.085 mW with two-level twisting. Fig. 5 shows that the untwisted geometry exhibits large differences among strand currents superposed on local dipolar patterns, while single-level twisting equalizes strands mainly within each bundle. Two-level twisting nearly suppresses the bundle- and strand-scale circulating currents, although the local proximity-current mode remains inside each strand.

Thus, the first twisting level mitigates most strand-scale imbalance under common-terminal voltage excitation. Under a transverse external field, however, single-level twisting leaves bundle-position-dependent differences in flux linkage. The second twisting level transposes the bundle positions and suppresses the resulting bundle-scale circulating currents.

IV. Conclusion

A voltage excitation formulation of the IEM was developed for Litz wire analysis with circulating currents and a uniform external magnetic field. The formulation explicitly assembles a strand-level impedance matrix to determine strand currents, while the external field is incorporated through direct induced voltages and the magnetization response. The formulation was validated using a four-conductor model and was demonstrated using three 49-strand Litz-wire geometries with 3-D twisting. The results showed that the twisting level required to suppress

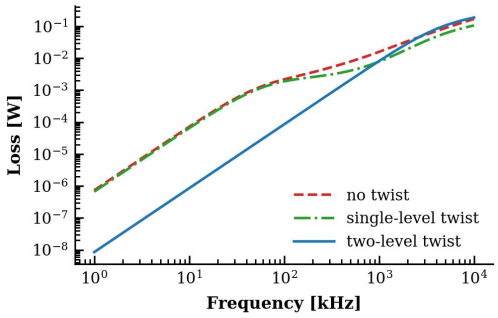

Fig. 4. Loss under a uniform 1-mT peak external field, zero applied voltage, and zero net terminal current.

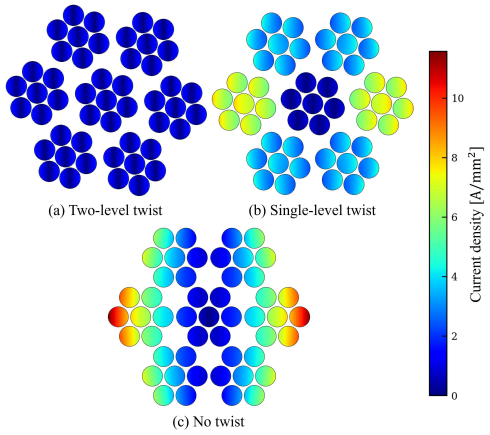

Fig. 5. Reconstructed current-density magnitude at 100 kHz under the 1-mT peak external field with zero applied voltage and zero net terminal current.

loss depends on the excitation mechanism. Full 3-D FEM or experimental validation and quantitative comparisons of computation time and memory usage with 3-D FEM remain future work.

References

[1] T. Guillod, J. Huber, F. Krismer, and J. W. Kolar, "Litz wire losses: Effects of twisting imperfections," in *Proc. IEEE 18th Workshop Control Model. Power Electron. (COMPEL)*, Jul. 2017, pp. 1–8.

[2] Y. Otomo, H. Igarashi, H. Sano, and T. Yamada, "Analysis of litz wire losses using homogenization-based FEM," *IEEE Trans. Magn.*, vol. 57, no. 8, Aug. 2021, Art. no. 7402409.

[3] S. Ehrlich, H. Rossmanith, M. Sauer, C. Joffe, and M. März, "Fast numerical power loss calculation for high-frequency litz wires," *IEEE Trans. Power Electron.*, vol. 36, no. 2, pp. 2018–2032, Feb. 2021.

[4] C. Liu *et al.*, "Three-dimensional semi-finite element-based proximity loss calculation for litz wires in a high-frequency transformer," *IEEE Trans. Ind. Appl.*, vol. 61, no. 1, pp. 560–571, Jan./Feb. 2025.

[5] R. Inoue, R. Takada, H. Ueda, and S. Kim, "Basic study on the structural design for large-capacity litz wires using an equivalent circuit model considering the path of all strands," in *Proc. IEEE Energy Convers. Congr. Expo. (ECCE)*, 2024, pp. 6933–6938.

[6] S. Hiruma and H. Igarashi, "Fast 3-D analysis of eddy current in litz wire using integral equation," *IEEE Trans. Magn.*, vol. 53, no. 6, Jun. 2017, Art. no. 7000704.

[7] S. Hiruma, Y. Otomo, and H. Igarashi, "Eddy current analysis of litz wire using homogenization-based FEM in conjunction with integral equation," *IEEE Trans. Magn.*, vol. 54, no. 3, Mar. 2018, Art. no. 7001404.

[8] H. Igarashi, "Semi-analytical approach for finite-element analysis of multi-turn coil considering skin and proximity effects," *IEEE Trans. Magn.*, vol. 53, no. 1, Jan. 2017, Art. no. 7400107.

[9] J. A. Ferreira, "Improved analytical modeling of conductive losses in magnetic components," *IEEE Trans. Power Electron.*, vol. 9, no. 1, pp. 127–131, Jan. 1994.